# Spontaneous Perpendicular Orientation of Cylindrical Microdomains in a Block Copolymer Thick Film

**Shinichi Sakurai,*,† Hiromichi Bando,† Hidekazu Yoshida,† Ryoko Fukuoka,‡ Masahiro Mouri,‡ Katsuhiro Yamamoto,§ and Shigeru Okamoto§**

*Department of Polymer Science & Engineering, Graduate School of Science and Technology, Kyoto Institute of Technology, Sakyo-ku, Kyoto 606-8585, Japan; Asahikasei Chemicals Co., Yako, Kawasaki-ku, Kawasaki 210-0863, Japan; and Department of Materials Science, Graduate School of Engineering, Nagoya Institute of Technology, Gokiso, Showa-ku, Nagoya 466-8555, Japan*

*Received April 11, 2008; Revised Manuscript Received January 30, 2009*

ABSTRACT: We show an unconscious self-assembling ability of block copolymers, that is, spontaneous perpendicular orientation of nanocylinders in a block copolymer thick film of polystyrene-*block*-polyethylenebutylene-*block*-polystyrene (SEBS) triblock copolymer. The perpendicular orientation of cylinders was obtained when the SEBS sample underwent morphological transition from spheres to cylinders, which was mediated by directional coalescence of spheres normal to the film sample. The direction of the cylinder orientation is determined already by the direction of the solvent evaporation, which can be referred to as an effect of a chemical potential gradient. We have not been aware of such self-assembling ability of block copolymers. Its robustness can be identified in a thick film (about 1 mm thickness), and it is expected that this opens up a wide use of block copolymers as a self-sustaining film in many practical applications.

## Introduction

Block copolymers undergo microphase separation in a few tens of nanometers because of strong segregation between constituent block chains comprising different chemical species.[1] This stems in molecular origins where dimension of block chains is of tens of nanometers. Depending on composition, the morphology of such a nanostructure can be altered as spheres, cylinders, double gyroid, or lamellae. It is well-known that physical properties of block copolymers strongly depend on the morphology. Not only the morphology but also the orientation of the nanostructures are key factors to be taken into account in order to control materials properties more efficiently, such as imparting anisotropy of properties. Controlling of orientation of the nanostructures[2] is therefore one of the fundamental ways to novel specialty materials.

There have been continuous attempts to orient nanocylinders of block copolymer perpendicular to its film sample. This is because such a film containing perpendicularly oriented nanocylinders will have excellent functions due to uniform diameter of cylinders in a few tens of nanometers. A selective etching on the cylinders gives a bunch of uniform nanopores passing through the film. Such a film can be used as a selective separation membrane and templates for nanowires and nanotubes. Generally, imposing a flow field[3−5] works well to orient cylindrical nanostructures such that the cylinders orient parallel to the flow. However, it is clear that this method fails for the perpendicular orientation due to deficiency of imposing flow field perpendicular to a film sample. Nevertheless, several methods are even available for the perpendicular orientation of cylinders, such as imposing an electric field to a film,[6,7] modification of substrate surface chemically or physically (topologically),[8,9] utilization of amphiphilic block copolymers comprising hydrophilic and hydrophobic chains,[10] or solvent evaporation-assisted perpendicular orientation of cylinders.[11−17] It is also known that spatial confinement causes perpendicular orientation of cylinders when thickness of the film is comparable to the repeat distance of cylinders.[18] Note, however, that these methods are limited for a thin film thinner than several micometers.

On the other hand, there is no report of perpendicular orientation of cylinders in a thick film (thickness in the 0.1−1.0 mm range). For this problem, a novel self-assembling ability of a block copolymer such as a directional coalescence of spherical nanostructures in the direction perpendicular to the film sample is required. The concept is schematically shown in Figure 1, where the resultant cylinders are spontaneously oriented perpendicularly due to a memory of the chemical potential gradient induced by solvent evaporation. If nonequilibrium spherical nanostructures, which can be obtained when a cylinder-forming block copolymer is cast from a solution in selective solvent,[19] are frozen in an as-cast film due to vitrification of one or both components of block species, thermal annealing of the sample above their glass transition temperatures can induce coalescence of nonequilibrium spheres. Just the

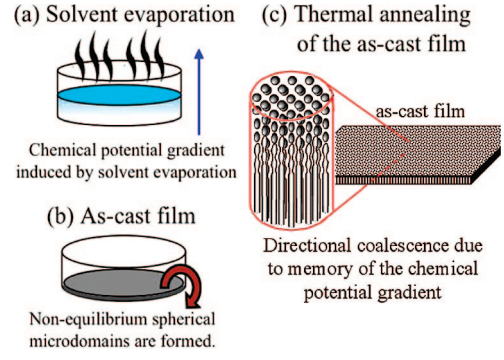


**Figure 1.** Schematic representation of the strategy used in this study for spontaneous orientation of nanocylinders normal to a block copolymer thick film. (a) Solvent evaporation process which induces the chemical potential gradient. (b) Nonequilibrium spherical microdomains formed in the as-cast film due to selective solvent used for the solution cast. (c) Directional coalescence of spherical microdomains perpendicular to the sample film, upon thermal annealing of the as-cast film above the glass transition temperature.

* Corresponding author. E-mail: shin@kit.jp.
† Kyoto Institute of Technology.
‡ Asahikasei Chemicals Co.
§ Nagoya Institute of Technology.

10.1021/ma900155n CCC: $40.75 
Published on Web 02/26/2009

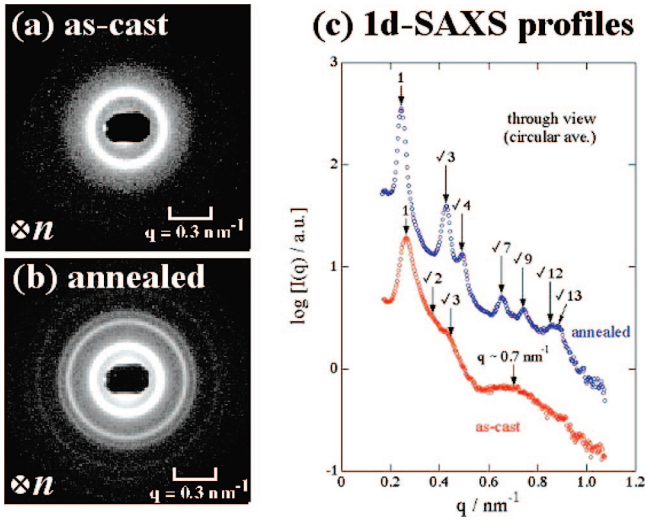


**Figure 2.** (a) Two-dimensional SAXS pattern (through view) for the as-cast film, (b) that for the annealed film (through view), both were measured at room temperature, and (c) corresponding one-dimensional SAXS profiles for the as-cast and annealed films. These profiles are obtained from the 2d-SAXS pattern by conducting circular average. ***n*** denotes unit vector normal to the film surface.

thermal annealing is very straightforward and convenient, as well, for the perpendicular orientation of cylinders. We show in this paper efficiency of this strategy using an SEBS (polystyrene-*block*-polyethylenebutylene-*block*-polystyrene) triblock copolymer.

## Experimental Section

The SEBS sample with the number-average molecular weight $M_n = 6.6 \times 10^4$ and the polydispersity index $M_w/M_n = 1.03$ was used. The volume fraction of polystyrene (PS) moiety is 0.16. Heptane, which is a good solvent of polyethylenebutylene (PEB) while poor for PS, was used for solution casting. However, it was not possible to prepare the heptane solution directly due to lack of solubility. To enhance solubility, dichloromethane, which is good for PS while poor for PEB, was used as a cosolvent, such that the 1:1 mixture of heptane/dichloromethane was actually used as the solvent. Since dichloromethane is volatile at room temperature, it evaporated rapidly from a 5% polymer solution. After complete evaporation of dichloromethane, heptane still remains. In this way, the heptane solution of SEBS was obtained. After complete evaporation of heptane (it took several days at room temperature (RT)), an as-cast film with 0.7 mm thickness was obtained, being subjected to thermal annealing at 210 °C for 3 h. Structural analyses were mainly conducted by two-dimensional small-angle X-ray scattering (2d-SAXS).

## Results and Discussion

Parts a and b of Figure 2 show 2d-SAXS patterns of through views for the as-cast and annealed films, respectively, where the incident X-ray beam is parallel to ***n***. Both patterns exhibit isotropic scattering. For precise structural analyses, we have conducted circular average of these isotropic 2d-SAXS patterns. Namely, the scattering intensity was averaged over the pixels with the same distance from the center of the 2d-SAXS pattern, irrespective of an azimuthal angle. The results of the circular average are shown in Figure 2c. The one-dimensional SAXS profile for the as-cast film exhibits a main peak at $q = 0.26$ nm$^{-1}$ ($q$ denotes the magnitude of the scattering vector as defined by $q = (4\pi/\lambda)\sin(\theta/2)$ with $\lambda$ and $\theta$ being the wavelength of X-ray and the scattering angle, respectively), which is a reflection of the {110} plane of the body-centered cubic lattice (bcc) of ordered PS nanospheres. Furthermore,

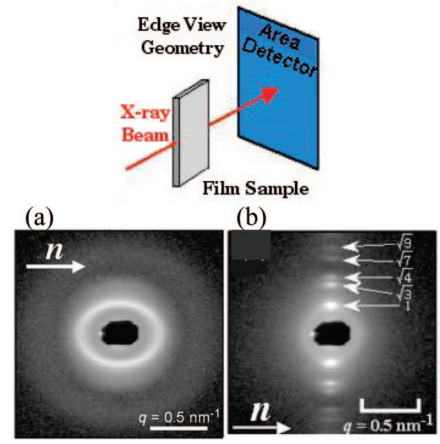


**Figure 3.** 2d-SAXS patterns of edge view for (a) as-cast and (b) annealed films.

higher-order reflections can be identified at relative $q$ positions of $\sqrt{2}$ and $\sqrt{3}$ multiples of the main peak position, which are reflections of {200} and {211} planes of the bcc lattice. Additionally, a broad peak is also observed at $q = 0.70$ nm$^{-1}$, which is ascribed to a form factor of the scattering. From the peak position ($q_m$), the radius ($R$) of the nanosphere can be evaluated by using the relation $R = 5.765/q_m$.[20] Thus, the radius was determined to be 8.2 nm for the PS nanospheres.

On the contrary, many reflection peaks are observed in the one-dimensional SAXS profile for the annealed sample. Their relative $q$ positions are 1, $\sqrt{3}$, $\sqrt{4}$, $\sqrt{7}$, $\sqrt{9}$, $\sqrt{12}$, and $\sqrt{13}$, which are reflections from $\{10\bar{1}0\}$, $\{11\bar{2}0\}$, $\{20\bar{2}0\}$, $\{21\bar{3}0\}$, $\{30\bar{3}0\}$, $\{22\bar{4}0\}$, and $\{31\bar{4}0\}$ planes of the hexagonal lattice for the PS nanocylinders in the PEB matrix. Therefore, it was confirmed that upon the thermal annealing the SEBS sample retrieved its equilibrium domain structures. This in turn indicates that the structures (PS nanospheres) formed in the as-cast film were nonequilibrium due to difference in solubility of PS and PEB moieties to heptane (solvent used for the solution cast). Since heptane is a good solvent for PEB while it is poor for PS, in the presence of heptane the effective volume fraction of the PS phase is much decreased, which can alter the morphology. It is actually considered that the PS phase shrinks into spheres in an early stage of the solution-cast process in the heptane solution. Note here that the cosolvent dichloromethane has evaporated in this stage. Upon the increase of the polymer concentration, the PS nanospheres are finally vitrified so that the SEBS sample cannot retrieve its equilibrium cylinder structures because of inhibition of coalescence of the glassy PS nanospheres. This scheme explains the fact that the PS nanospheres remained in the as-cast film after complete evaporation of heptane, although the structures are nonequilibrium.[21] The thermal annealing above the glass transition temperature of the PS phase unlocks the frozen state so that the SEBS sample could attain the equilibrium domain structures (PS nanocylinders). Thus, it turned out that upon the thermal annealing the PS nanospheres coalesced each other, transforming into PS nanocylinders.

Figure 3 shows 2d-SAXS patterns of edge views for the as-cast and annealed films. The geometrical relationship of the sample film and the X-ray detector for the edge view measurement is schematically shown together. Many reflection spots were observed at relative $q$ positions of 1, $\sqrt{3}$, $\sqrt{4}$, $\sqrt{7}$, and $\sqrt{9}$, being assigned to $\{10\bar{1}0\}$, $\{11\bar{2}0\}$, $\{20\bar{2}0\}$, $\{21\bar{3}0\}$, and $\{30\bar{3}0\}$ planes of the hexagonal lattice for cylinders. As seen in Figure 3b, the reflection spots were just in line along the meridian (perpendicular to ***n***). This means that all reflection planes with $l = 0$ are perpendicular to the film surface, indicating

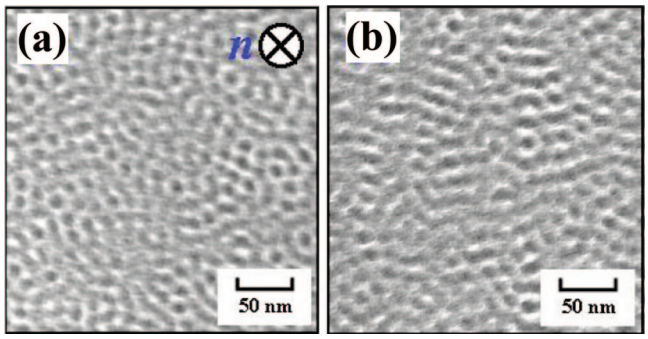


**Figure 4.** TEM micrographs for (a) through view image and (b) edge view image for the as-cast film. The PS domains are stained with $RuO_4$ and thus appear dark.

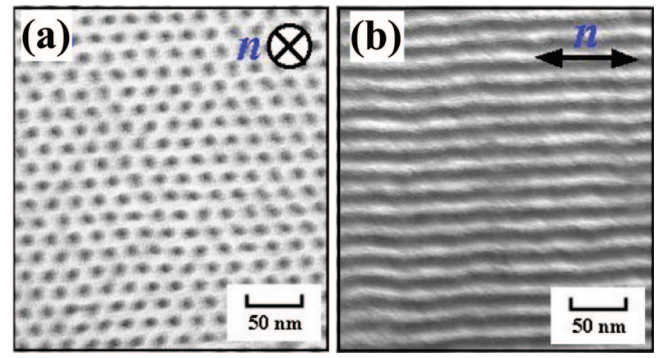


**Figure 5.** TEM micrographs for (a) through view image and (b) edge view image for the annealed film.

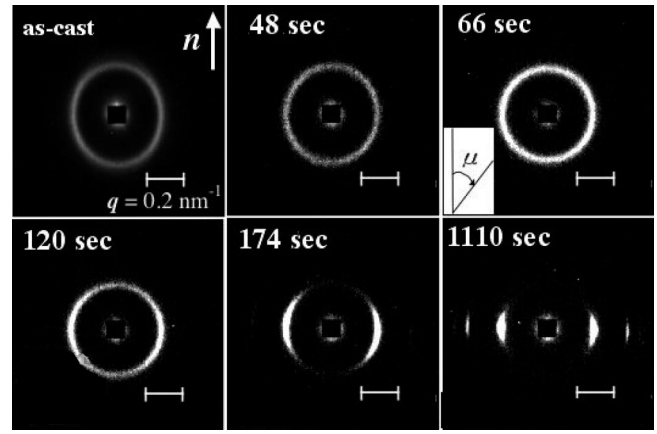


**Figure 6.** Changes in the 2d-SAXS pattern (edge view) with the annealing time upon temperature jump from room temperature to 225 °C. The measuring time at the each frame is 1.51 s. Definition of the azimuthal angle $\mu$ is shown together, as it is defined to increase in a clockwise manner with respect to the meridional vector pointing upward.

that the PS nanocylinders are all oriented perpendicularly. Namely, the post-transformed cylinders were spontaneously oriented normal to the film upon coalescence of the PS nanospheres.

We now confirm the SAXS results by transmission electron microscopy (TEM) for the as-cast and annealed films. Figure 4 shows the TEM micrographs for the as-cast film for (a) through and (b) edge views. The PS nanodomains are stained with $RuO_4$ so that they appear dark in the TEM micrographs, while the PEB nanodomains unstained appear bright. Unfortunately, the conventional TEM is not a powerful technique to figure out the morphology. It seems that the PS phase forms continuous domains but not spheres. This might be due to superposition of the cross-sectional views in the thickness direction. Actually, the average radius of the PS nanospheres is evaluated to be 8.2 nm, and the spacing of the {110} planes of the bcc lattice is 24.2 nm from the SAXS result, while the thickness of the ultrathin section subjected to the TEM observation is about 50 nm. Therefore, approximately several layers of the {110} planes are superposed. A special technique such as a TEM tomography is required for further confirmation. Nevertheless, it should be pointed out that many pieces of isolated spherical particles can be identified in the through view of the as-cast film as shown in Figure 4a, which may be in accord with the SAXS results. More interesting findings can be extracted from the edge view of the as-cast film shown in Figure 4b. Although the TEM observation is quite limited in a local area, it can be identified in the edge view that a linear alignment of the PS nanospheres is dominantly seen. The linear array of the PS nanospheres rather appears to be a coalesced wavy tube. Although we should be aware of the possibility of the superposition of the cross-sectional views in the thickness direction, such a wavy PS tube is indicative of a local coalescence of the PS nanospheres even during the solution casting. If such a wavy tube is approximately parallel to the film normal $\boldsymbol{n}$, it can be a guide of coalescence of the PS nanospheres, which in turn can nucleate spontaneous orientation of the post-transformed PS cylinders parallel to $\boldsymbol{n}$ (namely perpendicular to the film surface). Although such a wavy PS tube in the as-cast film may play a key role for the perpendicular orientation, the detection by SAXS is impossible due to its small population. The local area information can never be detected by SAXS. The 2d-SAXS pattern of the edge view shown in Figure 3a is a consequence of the most popular PS nanospheres. On the other hand, from Figure 5 showing the TEM micrographs for the annealed film for (a) through and (b) edge views, perpendicular orientation of PS nanocylinders, arranged locally in hexagonal lattice, is clearly confirmed.

Now we examine the experimental results more closely. The fact that the pattern in Figure 3a is distorted with longer axis parallel to $\boldsymbol{n}$ indicates that the domain spacing differs dependently on the azimuthal angle. Namely, the PS nanospheres are packed more closely in the vertical direction as compared to any other directions. This can be explained as follows: During the solvent evaporation, the spherical nanostructures are formed. At this moment, a large amount of solvent still remains. In the successive process, the solvent keeps evaporating and accordingly the thickness of the layer of the casting solution is reduced. Thus, the distance between the neighboring spheres decreases in the thickness direction (which is parallel to $\boldsymbol{n}$). On the other hand, the sample size of the lateral direction is fixed by the Petri dish side wall so that the distance between the neighboring spheres unchanges in the lateral direction (which is perpendicular to $\boldsymbol{n}$). Thus, the anisotropic arrangement of the PS spheres is formed in the as-cast film. This scheme further implies a local coalescence of the PS spheres, which gives rise to the wavy tubes, even during the solution casting. Such embryonic short cylinders (wavy tubes), if any, might orient parallel to $\boldsymbol{n}$ due to the solvent evaporation. This implies straightforwardly directional coalescence of the PS nanospheres in the vertical direction. However, we found experimentally that the elliptic 2d-SAXS pattern changed into an isotropic ring without coalescence upon heating above $T_g$ of PS. This is based on the experimental results as shown in Figure 6 where change in the 2d-SAXS pattern of the edge view with the annealing time upon temperature jump from RT to 225 °C is displayed. It was found that the spheres were completely transformed into cylinders at 174 s, as presented in Figure 7, which shows the 1d-SAXS profiles ($I(q)$ vs $q$) at 102 and 174 s elapsed. These were obtained by conducting a sector average in the vicinity of the equator. At 174 s, $\sqrt{3}$ and $\sqrt{4}$ peaks being ascribed to $\{11\bar{2}0\}$ and $\{20\bar{2}0\}$ reflection planes of the hexagonal lattice, respectively, are clearly

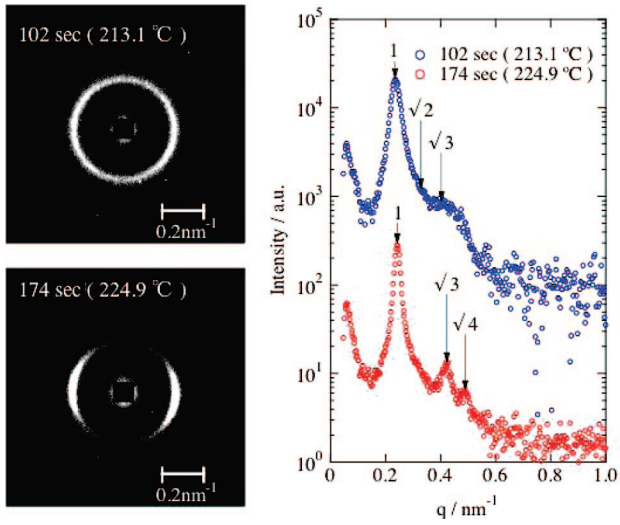


**Figure 7.** One-dimensional SAXS profiles obtained by conducting circular average of the 2d-SAXS patterns measured at 102 and 174 s elapsed from the onset of the T-jump.

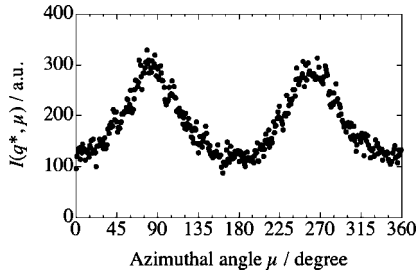


**Figure 8.** Plot of the SAXS intensity of the first-order peak, $I(q^*,\mu)$, as a function of the azimuthal angle $\mu$ for the 2d-SAXS pattern measured at 120 s elapsed. The definition of the azimuthal angle $\mu$ is shown in Figure 6.

seen. On the contrary, at 102 s elapsed, the 1d-SAXS profile showed $\sqrt{2}$ and $\sqrt{3}$ reflections from the bcc lattice of the spheres while the 2d-SAXS pattern became already isotropic. The transition from the elliptic shape to the isotropically round shape took place around 66 s (Figure 6), where the morphology was still spheres. These results indicate that the directional coalescence of spheres giving rise to perpendicularly oriented cylinders was not immediate and took place finally after a slightly prolonged annealing. Note further that sufficiently slow evaporation of solvent in the casting process resulted in a 2d-SAXS pattern, not being so distorted, for the as-cast film. However, even this case resulted in perpendicular orientation of cylinders. This fact implies that the shorter spacing between spheres in the direction parallel to $\boldsymbol{n}$ in the as-cast film is not a direct reason for the coalescence of spheres along $\boldsymbol{n}$.

Right after the transition, it was found that post-transformed cylinders already oriented perpendicularly, as shown in Figure 6 (174 s elapsed). To examine the degree of orientation, the integrated intensity of the first-order peak in the 1d-SAXS profile should be plotted as a function of the azimuthal angle $\mu$, where $\mu$ is defined to increase in a clockwise manner with respect to the meridional vector pointing upward (as shown in Figure 6). As an example, such a plot is shown in Figure 8 for the result obtained at 120 s elapsed. Symmetric distribution of the scattering intensity with respect to $\mu = 0°$ and 180° ensures an isotropic orientation distribution of cylinder axes around $\boldsymbol{n}$ (i.e., axisymmetry). For this case, the second-order orientation factor, $F_2$, can be given by[22]

$$F_2 = C^{-1}\frac{3\langle\cos^2\mu\rangle - 1}{2} \tag{1}$$

where the averaging on the term $\cos^2\mu$ is conducted as follows:

$$\langle\cos^2\mu\rangle = \int_0^{\pi}\cos^2\mu P(\mu)\sin\mu\,d\mu \tag{2}$$

with

$$P(\mu) = \frac{I(q^*,\mu)}{\int_0^{\pi} I(q^*,\mu)\sin\mu\,d\mu} \tag{3}$$

where $I(q^*)$ denotes the scattering intensity at $q = q^*$ for the first-order peak. The constant $C$ in eq 1 is attributed to geometric relationship of the probe orientation (with the angle $\Phi$) with respect to the cylinder axis and is given by

$$C = \frac{3\cos^2\Phi - 1}{2} = -\frac{1}{2} \quad \left(\Phi = \frac{\pi}{2}\right) \tag{4}$$

Since the first-order reflection spots appear in the $\boldsymbol{q}$ direction perpendicular to the $\{10\bar{1}0\}$ reflection plane (and in turn perpendicular to the cylinder axis), $\Phi$ equals to 90°, giving rise to $C = -1/2$. Division by the constant term $C$ in eq 1 ensures $F_2 = 1$ for the perfect perpendicular orientation of cylinders. Note here $F_2 = -2$ for the parallel orientation (the orientation angle zero with respect to the film surface) and $F_2 = 0$ for random orientation.

The thus-evaluated orientation factor is plotted against the annealing time in Figure 9 with open circles. Although it was found that spheres and cylinders coexisted in the range from 102 to 174 s, the orientation factor was evaluated directly from the raw 2d-SAXS results, on which the individual contributions (2d-SAXS patterns) from spheres and cylinders superposed. Therefore, to reveal the orientation factor of post-transformed cylinders, it is required to decompose the 2d-SAXS pattern into the individual contributions from spheres and cylinders. The decomposition was performed as follows. We assume that the first-order peak in the 1d-SAXS profile in between 102 and 174 s consists of the first-order peak from spheres and that from cylinders because it was found that the position of the first-order peak ($q$ value) for the spheres (at 102 s) slightly differs from that for cylinders (at 174 s) (see Figure 7) and also found that the first-order peak became gradually sharper with shifting positions toward higher $q$ from 102 to 174 s. Therefore, we conducted computational decomposition of the apparently single first-order peak into two peaks with the positions fixed at the one observed at 102 s and the other observed at 174 s by assuming that the former is the contribution from spheres and the latter from cylinders. Thus, the peak intensity for the individual contribution was estimated for every azimuthal angle, based on which the orientation factor was finally evaluated individually for spheres and cylinders.

The thus-evaluated orientation factor for cylinders in the coexisting time range is shown together in Figure 9 with filled circles. Note here that the open circles plotted in the range below 102 s indicate the orientation factor for {110} planes of the bcc lattice of spheres. The nonzero value of the orientation factor at 102 s (~0.12) suggests that the orientation of the bcc spheres is not uniform but rather preferential in the vertical direction. For simplicity, let us assume here that (110) planes are parallel to the film normal $\boldsymbol{n}$ and $[1\bar{1}1]$ directions parallel to $\boldsymbol{n}$ as well. Note here that a $[1\bar{1}1]$ direction places on a (110) plane. Since the nearest-neighboring spheres, which are subjected to coalesce each other, align in the $[1\bar{1}1]$ direction, the above-mentioned result indicates that the $[1\bar{1}1]$ direction parallel to the film normal overwhelms other $\langle 111\rangle$ directions, i.e., [111] and $[11\bar{1}]$ direc-

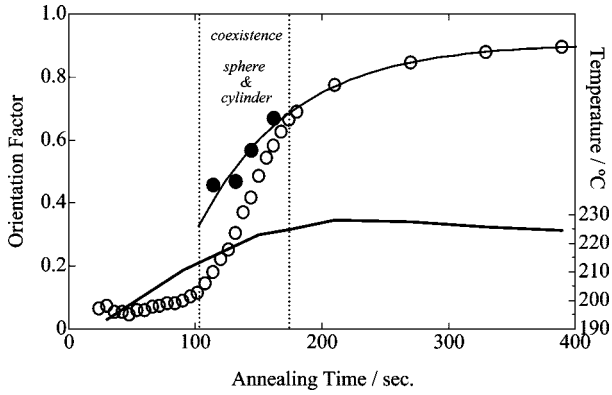


**Figure 9.** Variation of the orientation factor as a function of the annealing time upon temperature jump from room temperature to 225 °C. The values were evaluated from the results of the 2d-SAXS measurements shown in Figure 6. Open circles indicate the orientation factor evaluated using the raw data of 2d-SAXS, while closed circles show the orientation factor for the individual contribution of cylinders in the range from 102 to 174 s, where spheres and cylinders coexisted. To evaluate the individual contribution peak decomposition of the SAXS data was appropriately conducted (see the text for more details).

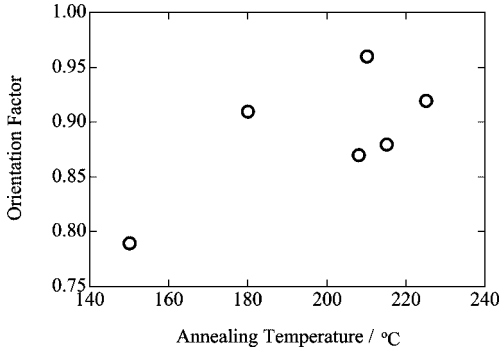


**Figure 10.** Attainable orientation factor as a function of the annealing temperature in the range from 140 to 225 °C.

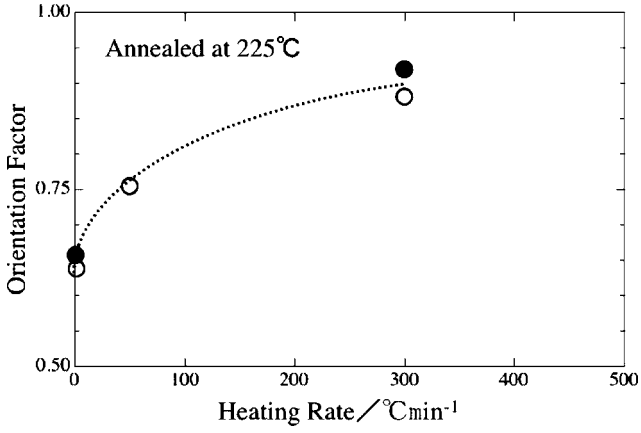


**Figure 11.** Attainable orientation factor as a function of the heating rate, where the final destination temperature is 225 °C. Open symbol indicates the result obtained at room temperature for the sample subjected to the thermal annealing from 100 to 225 °C with a given heating rate. The samples were rapidly quenched to room temperature right after reaching 225 °C. On the other hand, closed symbols show the result obtained at 225 °C during heating with the rates of 0.8 °C/min and the result obtained aftert a T-jump experiment from 100 to 225 °C (the heating rate for this experiment is approximated as 300 °C/min).

tions (not on the (110) plane) as well as the $[\bar{1}11]$ direction (on the (110) planes) by population. This can be considered as a memory of the solvent evaporation in the casting process and may be a trigger to the successive spontaneous perpendicular orientation of the post-transformed cylinders. As a matter of fact, the orientation factor of the post-transformed cylinders around 102 s is as large as 0.48, which means they were already oriented in the direction of the film normal. The discontinuous jump of the orientation factor from 0.12 to 0.48 upon the transformation from spheres to cylinders at 102 s is quite significant. This fact further suggests that the $[1\bar{1}1]$ direction parallel to the film normal is preferentially selected as the direction of the coalescence of spheres.

We should then explain the reason why one of the $\langle 111 \rangle$ directions, which is the $[1\bar{1}1]$ direction in the particular discussion above made, aligns parallel to the film normal $\boldsymbol{n}$. Let us start considering the reported case of a thin film, for which solvent evaporation can induce perpendicular orientation of cylinders.[6,9,16,17] This is due to permeation (migration) path of solvent, through which solvent molecules are transported toward the top surface of the solution.[17] Since cylinders should not block migration paths, orientation of cylinders parallel to them is resulted during solvent evaporation. Ho et al.[17] have proposed this kind of mechanism while Russell et al.[16] have proposed a different one. The latter is similar to a classical zone refinement where the ordering front grows from the surface of the casting solution and proceeds downward toward the bottom of the solution, which is mediated by the gradient of the solvent concentration. Since this kind of mechanism is not applicable to the case of a thick film, we have adopted the mechanism proposed by Ho et al.[17] Note however that the scheme proposed by Ho et al. is not applicable either for the case of the thick film because cylinders favor orientation parallel to the substrate. As for the case of spheres, a similar idea is applicable; the slip direction $[1\bar{1}1]$ of the bcc lattice is forced parallel to migration paths. Since the slip direction in the as-cast film is so controlled normal to the film by the solvent evaporation, the perpendicular orientation of cylinders through directional coalescence is not stochastic but deterministic. Failing of direct perpendicular orientation of cylinders in the case of the thick film reminds that the strategy we employed here is quite sophisticated.

We now discuss the manner of temporal evolution of the perpendicular orientation of cylinders. A single-exponential function can be fitted to the temporal change in the orientation factor beyond 102 s (in the successive process after the onset of the transition from spheres to cylinders), which is shown with a thin solid curve in Figure 9. The incompleteness of T-jump, which is also shown in Figure 9 with a thick solid curve, may affect the results. However, the temperature difference between 102 s (213.1 °C) and the final destination temperature (225.0 °C) is only −2.4% in Kelvin so that an unfavorable effect, if any, would be trivial. The fact that the temporal change in the orientation factor for the cylinders can be fitted by a single-exponential function indicates that temporal evolution of the perpendicular orientation of cylinders is a self-improving process, started from weakly oriented cylinders as transformed from spheres with weak orientation of the $[1\bar{1}1]$ directions of the bcc lattice. Namely, it is considered that weakly oriented cylinders or in other words embryonic wavy tubes play roles as a guideline of the spontaneous cylinder orientation perpendicular to the film surface.

We found that the finally attained orientation factor upon the T-jump to 225 °C is 0.92 at 1110 s elapsed (though it is not shown in Figure 9). It is interesting to reveal whether attainable orientation depends on the annealing temperature or not. Figure 10 shows the results. It can be concluded that the perpendicular orientation of the cylinders proceeds more when the annealing temperature is more elevated in the range from 150 to 225 °C. Note here that no transformation into cylinders was observed

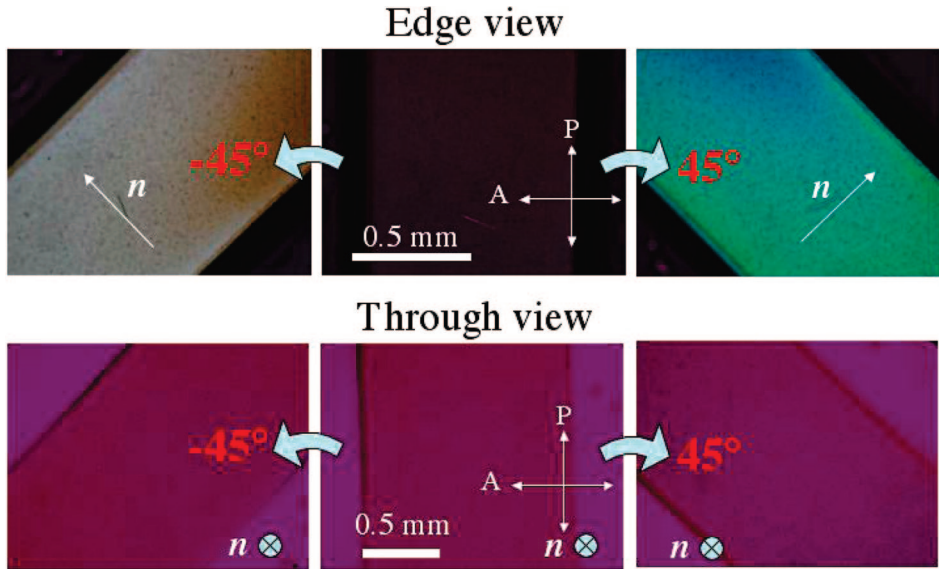


**Figure 12.** Polarizing optical micrographs obtained at room temperature for the samples annealed at 210 °C for 3 h under the crossed polarizing condition. A 530 nm retardation plate was inserted in between polarizer and analyzer. For the edge view observations, a thin-sliced sample (thickness was 0.2 mm) was used. Two cases of rotation angles between the cylinder axis and polarizer, −45° and +45°, are displayed for the through and edge views. For the through view, the thickness was 0.7 mm.

when the sample was thermally annealed at 140 °C for several hours. This result is amazing because the annealing temperature is much higher as compared to the glass transition temperature of the PS spheres. Although the transition from spheres to cylinders seemed to be governed simply by mobility of PS chains, the fact that the transition did not occur at 140 °C suggests that this is not the case. Rather, it can be considered that there might be a kinetic energy barrier of the transition.

The results shown in Figure 10 suggest that gradual transformation of spheres into cylinders cannot result in higher orientation of cylinders. To confirm this speculation, we examined the effect of the annealing rate on the orientation factor. Figure 11 shows the attainable orientation factor as a function of the heating rate, where the final destination temperature is 225 °C. This result clearly indicates that the perpendicular orientation finally attained becomes better when the annealing rate is faster even if the annealing temperature is the same. Thus, it is confirmed that sufficiently quick transformation of spheres into cylinders is required for the spontaneous cylinder orientation.

Among nanostructures of block copolymers, cylindrical or lamellar structure can be utilized for performance of anisotropic properties due to their anisotropic shape. For instance, refractive indices parallel and perpendicular to the anisotropic particle are different from each other, giving rise to the so-called form birefringence.[23] Actually, perpendicular orientation of cylinders imparts a singular value of the refractive index normal to the film. To confirm significant optical anisotropy, we performed the polarizing optical microscopic (POM) observation under crossed polarizing conditions at room temperature for the annealed sample. A 530 nm retardation plate was inserted in between polarizer and analyzer. For the edge view observation, a thin-sliced sample with thickness of 0.2 mm was used. Two cases of rotation, −45° and +45° (the angle is between cylinder axis and the analyzer), were displayed in Figure 12, where almost homogeneous bright colors were observed in the thorough area (grey for −45°, while light green for +45°). On the other hand, no retardation was found for the through view (thickness was 0.7 mm). Thus, the perpendicular orientation of cylinders provides optical anisotropy. From the color of POM edge views, the optical retardation $\Gamma$ ($= d\Delta n$; $d$ is the optical path length and $\Delta n$ is the birefringence) was evaluated 220 nm for $d = 0.2$ mm, giving $\Delta n = 1.10 \times 10^{-3}$. Order estimation gives $\Delta n = 1.25 \times 10^{-3}$ for the form birefringence of PS cylinders embedded in the PEB matrix, which closely matches with the experimentally obtained value (see below for the order estimation). This in turn ensures almost perfect perpendicular orientation.

According to the literature,[23] values of refractive index parallel and perpendicular to the cylinder axis ($n_{||}$ and $n_{\perp}$) can be evaluated.

$$n_{||}^{\,2} = \phi_p n_p^{\,2} + (1 - \phi_p) n_m^{\,2} \tag{5}$$

and

$$n_{\perp} = n_m \sqrt{\frac{(1 + \phi_p) n_p^{\,2} + (1 - \phi_p) n_m^{\,2}}{(1 + \phi_p) n_m^{\,2} + (1 - \phi_p) n_p^{\,2}}} \tag{6}$$

where $n_p$ and $n_m$ stand for the refractive indices of materials composing inside (cylindrical particle) and outside (matrix) of the cylinder, respectively, and $\phi_p$ denotes the volume fraction of cylinder. Since the literature value of the refractive index is not available for PEB, that of the poly(ethylene propylene) (PEP) was used instead. Namely, $n_p = n_{PS} = 1.5920$ and $n_m = n_{PEP} = 1.4748$ were adopted from the literature[24] ($\phi_p = 0.16$, $\phi_m = 0.84$). As a result, $n_{||} = 1.49417$ and $n_{\perp} = 1.49292$ were evaluated, giving rise to the extent of the form birefringence $\Delta n = n_{||} - n_{\perp} = 1.25 \times 10^{-3}$. Although the extent is less than the intrinsic birefringence of a polymer chain (typically less than 2 orders of magnitude), it is not negligible.

## Concluding Remarks

In conclusion, we find a novel, fascinating, and sophisticated mechanism of spontaneous perpendicular orientation of nanocylinders in a thick block copolymer film through directional coalescence of spheres. Since the mechanism is controlled simply by the solvent evaporation, the corresponding process to produce such a film containing perpendicularly oriented nanocylinders can be much simplified, just the thermal annealing of the as-cast film! Anisotropic properties can be extracted from this film material. As an example, an anisotropic optical property is presented where perpendicular orientation of cylinders imparts

a singular value of the refractive index normal to the film. This can be utilized for production of a peculiar optical film. Anisotropic mechanical properties will also be useful. When the film consists of hard (PS) cylinders and soft (PEB) matrix, the same as that used in this study, it is expected that the film is 2-dimensionally soft for stretching but quite tough against compression. Inversely, if the film comprises the soft (PEB) cylinders embedded in the hard (PS) matrix, it will be 2-dimensionally ductile for the elongation parallel to the film surface, which can be utilized as a 2-dimensional shrinkable film. More tremendous applications are expected.

Although it deserves an important future work to confirm whether the concept for the perpendicular orientation of cylinders shown in Figure 1 can be applied to a thin film, we have conducted the SAXS measurements and have confirmed that the perpendicular orientation of the cylinders was formed in the film with 10 $\mu$m thickness, while for the 5 $\mu$m thickness the orientation was not perpendicular nor parallel to the substrate. Therefore, it should be stated that the proposed mechanism is only valid for a film thicker than 10 $\mu$m for this particular sample.

**Acknowledgment.** This work is supported in part by the Grant-in-aid from the Japanese Ministry of Education, Culture, Science and Sport (15350134 granted to S.S. and 17550189 granted to S.O.). The SAXS experiments were performed at the Photon Factory of the High Energy Accelerator Research Organization (Approval 2005G187) and at SPring-8 (Approval 2005B0383-NL2-np). We thank technical support for the SAXS experiments from Drs. Hara and Sugino at the Nagoya Institute of Technology. This work was partially supported by ISS Applied Research Partnership Program.

## References and Notes

(1) Sakurai, S.; Okamoto, S.; Sakurai, K. *Developments in Block Copolymer Science and Technology*; Hamley, I. W., Ed.; John Wiley & Sons: Chichester, England, 2004; Chapter 4.
(2) Sakurai, S. *Polymer***2008**, *49*, 2781.
(3) Chen, Z.-R.; Chen Kornfield, J. A.; Smith, S. D.; Grothaus, J. T.; Satkowski, M. M. *Science* **1997**, *277*, 1248.
(4) Watanabe, H. In *Structure and Properties of Multi-Phase Polymeric Materials*; Araki, T., Tran-Cong, Q., Shibayama, M., Eds.; Marcel Dekker: New York, 1998; Chapter 9.
(5) Sakurai, S.; Kota, T.; Isobe, D.; Okamoto, S.; Sakurai, K.; Ono, T.; Imaizumi, K.; Nomura, S. *J. Macromol. Sci., Phys.* **2004**, *B43*, 1.
(6) Morkved, T. L.; Lu, M.; Urbas, A. M.; Ehrichs, E. E.; Jaeger, H. M.; Mansky, P.; Russell, T. P. *Science* **1996**, *273*, 931.
(7) Thurn-Albrecht, T.; Schotter, J.; Kästle, G. A.; Emley, N.; Shibauchi, T.; Krusin-Elbaum, L.; Guarini, K.; Black, C. T.; Tuominen, M. T.; Russell, T. P. *Science* **2000**, *290*, 2126.
(8) Shin, K.; Leach, K. A.; Goldbach, J. T.; Kim, D. H.; Jho, J. Y.; Tuominen, M.; Hawker, C. J.; Russell, T. P. *Nano Lett.* **2002**, *2*, 933.
(9) (a) Sivaniah, E.; Hayashi, Y.; Iino, M.; Hashimoto, T. *Macromolecules* **2003**, *36*, 5894. (b) Sivaniah, E.; Hayashi, Y.; Matsubara, S.; Kiyono, S.; Hashimoto, T.; Fukunaga, K.; Kramer, E. J.; Mates, T. *Macromolecules* **2005**, *38*, 1837.
(10) (a) Watanabe, K.; Yoshida, H.; Kamata, K.; Iyoda, T. *Trans. Mater. Res. Soc. Jpn.* **2005**, *30*, 377. (b) Morikawa, Y.; Nagano, S.; Watanabe, K.; Kamata, K.; Iyoda, T.; Seki, T. *Adv. Mater.* **2006**, *18*, 883.
(11) Turturro, A.; Gattiglia, E.; Vacca, P.; Viola, G. T. *Polymer* **1995**, *36*, 3987.
(12) Mansky, P.; Chaikin, P.; Thomas, E. L. *J. Mater. Sci.* **1995**, *30*, 1987.
(13) Mansky, P.; Harrison, C. K.; Chaikin, P. M.; Register, R. A.; Yao, N. *Appl. Phys. Lett.* **1996**, *68*, 2586.
(14) Kim, G.; Libera, M. *Macromolecules* **1998**, *31*, 2569.
(15) Lin, Z.; Kim, D. H.; Boosahda, L.; Stone, D.; LaRose, L.; Russell, T. P. *Adv. Mater.* **2002**, *14*, 1373.
(16) Kim, S. H.; Misner, M. J.; Xu, T.; Kimura, M.; Russell, T. P. *Adv. Mater.* **2004**, *16*, 226.
(17) Ho, R. M.; Tseng, W. H.; Fan, H. W.; Chiang, Y. W.; Lin, C. C.; Ko, B. T.; Huang, B. H. *Polymer* **2005**, *46*, 9362.
(18) van Dijk, M. A.; van den Berg, R. *Macromolecules* **1995**, *28*, 6773.
(19) Sakurai, S.; Momii, T.; Taie, K.; Shibayama, M.; Nomura, S.; Hashimoto, T. *Macromolecules* **1993**, *26*, 485.
(20) Tanaka, H.; Hasegawa, H.; Hashimoto, T. *Macromolecules* **1991**, *24*, 240.
(21) It has been reported that thermoreversible transition between face-centered cubic (fcc) structure and bcc is available for spherical micelles in block copolymer solutions with selective solvents.[25] This suggests that fcc has a chance to be frozen in the as-cast film. The one-dimensional SAXS profile shown in Figure 2c lacks the second-order reflection peak of fcc at $q = 1.15q^*$ ($q^*$: position of the first-order peak), which is the reflection from the {200} planes of fcc, the possibility of the fcc can be ruled out. However, there would be still a chance to consider possibility of the transition from fcc to bcc as the solvent evaporation proceeds in our system.
(22) Sakurai, S.; Aida, S.; Okamoto, S.; Ono, T.; Imaizumi, K.; Nomura, S. *Macromolecules* **2001**, *34*, 3672.
(23) Folkes, M. J.; Keller, A. *Polymer* **1971**, *12*, 222.
(24) Brandrup, J.; Immergut, E. H. *Polymer Handbook*, 3rd ed.; John Wiley & Sons: New York, 1989; pp VI/459−VI/460.
(25) (a) Bang, J.; Lodge, T. P.; Wang, X.; Brinker, K. L.; Burghardt, W. R. *Phys. Rev. Lett.* **2002**, *89*, 215505. (b) Lodge, T. P.; Bang, J.; Park, M. J.; Char, K. *Phys. Rev. Lett.* **2004**, *92*, 145501.

MA900155N